submitted to *Geophys. J. Int.*

Comparison analysis of the ETAS model with Gutenberg-Richter (GR), Tapered-GR and Characteristic magnitude distributions

I. Spassiani[1⋆], S. Yaghmaei-Sabegh[2], R. Console[3,1], G. Falcone[1], M. Murru[1]

[1] *Istituto Nazionale di Geofisica e Vulcanologia (INGV), Rome, Italy*

[2] *University of Tabriz, Department of Civil Engineering, Tabriz, Iran*

[3] *Center of Integrated Geomorphology for the Mediterranean Area, Potenza, Italy*

SUMMARY

In this paper, we carry out a comparison analysis of the Epidemic Type Aftershock Sequence (ETAS) model for the earthquake process, embedded with the three main exponential-type distributions adopted in practical applications to describe the magnitudes of seismic events, that are, the Gutenberg-Richter (GR), the tapered Gutenberg-Richter (TGR) and the CHaracteristic (CH) frequency-magnitude distributions (FMDs). The first law is a pure-power decreasing function, while both the other two introduce a more rapid decay in the tail of the distribution: a soft taper in the TGR model and a sharp cutoff in the CH one. To perform the comparison, we first investigate some theoretical features of the ETAS model with CH-distributed magnitudes (ETAS-CH), which have not been deeply analyzed in the literature as much as for ETAS-TGR and ETAS-GR. In particular, we explicitly compute the branching ratio, we analyze its asymptotics in relation to its parameters, and we derive the proper stability conditions. We then move to the comparison among the three ETAS-GR, ETAS-TGR and ETAS-CH processes, to highlight differences and similarities. This is done by carrying out both a theoretical analysis, mainly focused on the three models' branching ratios and the relative sensitivity, and a simulation analy-

sis of realistic synthetic catalogs to compare the processes' numbers, events' magnitude distribution and temporal evolution. The results we obtained show that the ETAS-TGR and ETAS-CH processes have very similar features. They both have also less restrictive non-explosion conditions than for ETAS-GR; in fact, differently from this latter case, their branching ratios exist for any value of the parameters and are lower than the one of ETAS-GR, to which they converge for large magnitudes.

Key words: Statistical seismology, Statistical methods, Probability distributions.

1 INTRODUCTION

The magnitudes of seismic events in statistical seismology applications are typically modeled like exponential-type random variables. The most used Frequency-Magnitude Distribution (FMD) is indeed the Gutenberg-Richter (GR) law (Gutenberg & Richter 1944), which is a decreasing exponential distribution according to which the number N of events with a magnitude $\geq m$ is given by $N(m) = 10^{a-b(m-m_t)}$, where m_t is the completeness threshold and a, b are two positive parameters. The first one characterizes the seismic activity (earthquake productivity) in a given region and precisely represents the number of events above the completeness magnitude. The second parameter is instead the so-called b-value and describes the ratio of the smaller events with respect to the larger ones. Great interest has been shown by the scientific community to this parameter, which is debated to vary in space and/or time, thus suggesting its interpretation in terms of a physical process providing important information about the crustal tectonics (Westerhaus et al. 2002; Montuori et al. 2010; Hussain et al. 2020; Arroyo-Solórzano & Linkimer 2021). This discussion is still active in the literature, and the main criticisms are ascribed to the fact that the b-value estimation is susceptible to several sources of bias (Marzocchi et al. 2020).

Although the GR law is a benchmark in practical seismological applications, some investigations have highlighted that it may not be appropriate in a complete earthquake catalog for near fault regions (e.g., Ishibe & Shimazaki (2008); Field et al. (2017)), where it has been shown to overestimate the probability of large earthquake magnitudes. Various alternatives have therefore been proposed to account for the limited amount of stress energy in small domains, or for the finiteness of the seismic moment flux and the deformational energy (Kagan 2002; Schorlemmer et al. 2005; Tan et al. 2019). Among them, the most used ones are the Tapered (Pareto) Gutenberg-Richter (TGR) law, and the

⋆ Corresponding author

Characteristic (CH) model, both accommodating a change from a power law to a more rapid decay: the first as an exponential taper which varies with the magnitude, the second as a sharp cutoff (Kagan 2002). The main difference is that the GR simple power-law scaling relationship is adapted to have a lower or null (respectively in the case of TGR or CH) probability of strong events to occurr (more precisely, events stronger than a fixed threshold). Several studies have been made to show the main features of each model and to capture source seismicity in b-value estimation and seismic hazard analysis results (Kagan et al. 2010; Spassiani & Marzocchi 2021; Taroni et al. 2021; Yaghmaei-Sabegh & Ebrahimi-Aghabagher 2017; Yaghmaei-Sabegh & Ostadi-Asl 2021). Some direct comparisons have already been performed between GR and one of the other two distributions for practical cases. Wesnousky (1994) used paleoearthquake and fault slip-rate to examine the shape of FMDs in Southern California; Ishibe & Shimazaki (2012) used a high quality catalog compiled by the Japan Meteorological Agency (JMA) to show whether the GR or CH models more adequately describe the FMD around late Quaternary active faults; Spassiani & Marzocchi (2021) introduced a modification in the TGR distribution to obtain an optimal fit for seismicity in small spatiotemporal domains, and showed a practical application to the $M_w 7.3$ Landers earthquake occurred in California in 1992.

In order to delve into the models' differences, in this paper we compare the three FMDs of GR, TGR and CH all together. Throughout the text, we will use this terminology for consistency with the paper by Kagan (2002), which is a reference work in the literature. To do the comparison, we firstly give the formal definition of the probability density functions (PDFs) in terms of the seismic moments (hereafter indicated with capital letter M), instead of the magnitudes (hereafter indicated with small letter m), as in this way the definitions are more readable and the theoretical comparison is more straightforward. More precisely, we use the relation $M = 10^{\frac{3}{2}m+9}$ (M measured in Nm) by Kanamori (1977) which links the two quantities in a unique, bijective way. The PDFs of GR, TGR and CH can then be written as:

$$\phi_{GR}(M) = \beta_k M_t^{\beta_k} M^{-1-\beta_k} \qquad M_t \leq M, \tag{1}$$

$$\phi_{TGR}(M) = \left[\frac{\beta_k}{M} + \frac{1}{M_c}\right] \left(\frac{M}{M_t}\right)^{-\beta_k} \exp\left\{\frac{M_t - M}{M_c}\right\} \qquad M_t \leq M, \tag{2}$$

$$\phi_{CH}(M) = \beta_k M_t^{\beta_k} M^{-1-\beta_k} + \delta\,(M - M_{xc}) \left(\frac{M_t}{M_{xc}}\right)^{\beta_k} \qquad M_t \leq M \leq M_{xc}, \tag{3}$$

where: M_t is the seismic moment of completeness; $\beta_k = \frac{2}{3}b$; M_c controls the upper range distribution

in the TGR law; M_{xc} is the upper bound seismic moment of the CH distribution; $\delta(\cdot)$ is the Dirac delta function.

To the aim of modeling the entire earthquake sequence, the FMD is usually embedded in a stochastic process that involves also spatial and temporal components. The most used one is the Epidemic Type Aftershock Sequence (ETAS) model, a benchmark in statistical seismology consisting in a branching, clustering process of events evolving in successive generations (Ogata 1988, 1998; Console & Murru 2001; Console et al. 2003; Zhuang 2012). Its conditional intensity, that completely characterizes the process, dependes on the Omori-Utsu law for the aftershocks temporal decay, on a spatial kernel for the earthquakes location distribution and on the productivity law $\varrho(M) = \kappa \left(\frac{M}{M_t}\right)^{\alpha_k}$, here written in terms of the seismic moment, which represents the expected number of aftershocks triggered by a given mother event (κ, α_k are positive parameters, and $\alpha_k = \frac{2}{3}\alpha$, where α is the fertility exponent parameter of the productivity law written in terms of the magnitudes).

The stability of the ETAS process, that is the non-explosion of the seismic sequence it models, is assessed by looking at the relative branching ratio η, that is the integral

$$\eta = \int_{M_t}^{\infty} \phi(x)\varrho(x)dx, \tag{4}$$

where $\phi(\cdot)$ is the generic FMD. The branching ratio is indeed the proportion of triggered events with respect to all the shocks. De facto, this quantity corresponds to the critical parameter of the process, i.e. the average number of first-generation shocks per mother event. It then follows that it has to be set lower than 1 for the process not to explode.

The branching ratios η_{GR} and η_{TGR} for the ETAS model with GR- and TGR-distributed magnitudes (hereafter, ETAS-GR and ETAS-TGR, respectively) can be explicitly and straightforwardly computed as shown in Zhuang et al. (2012) and Spassiani (2021), obtaining:

$$\eta_{GR} = \frac{\kappa\beta_k}{\beta_k - \alpha_k}, \quad \beta_k > \alpha_k, \tag{5}$$

$$\eta_{TGR} = \kappa + \kappa\alpha_k \ \exp\left\{\frac{M_t}{M_c}\right\} \left(\frac{M_t}{M_c}\right)^{\beta_k - \alpha_k} \Gamma\left(-\beta_k + \alpha_k, \frac{M_t}{M_c}\right), \tag{6}$$

where we recall that κ concerns the earthquake productivity, and $\Gamma(s,t) = \int_t^{\infty} y^{s-1}e^{-y}dy$ is the upper incomplete Gamma function. We stress that η_{GR} can be computed only for $\beta_k > \alpha_k$ in order for the integral (4) to converge. Instead, this condition is relaxed for η_{TGR} where the taper impeds the number of events to become infinite (Spassiani 2021). When $\beta_k = \alpha_k$, we can in fact more simply rewrite the ETAS-TGR branching ratio as

$$\eta_{TGR,\,\beta_k=\alpha_k} = \kappa + \kappa\beta_k \ \exp\left\{\frac{M_t}{M_c}\right\} E_1\left(\frac{M_t}{M_c}\right), \tag{7}$$

where $E_1(z) = \int_z^\infty \frac{e^{-t}}{t} dt$ is the exponential integral.

In what follows, we will first focus on the theoretical analysis of the ETAS-CH process, so far not deeply studied in the literature. More precisely, we firstly explicitly derive the branching ratio, then we perform a sensitivity analysis with respect to its parameters, and finally we investigate the process stability. We then move to the comparison among the three ETAS-GR, ETAS-TGR and ETAS-CH processes, by focusing mainly on the relative FMDs and branching parameters η_{GR}, η_{TGR} and η_{CH}, through both a theoretical and a simulation analysis.

2 BRANCHING RATIO OF THE ETAS-CH PROCESS

To the aim of computing the branching ratio of the ETAS model with CH-distributed magnitudes (ETAS-CH), we substitute the expression (3) in the integral (4). A straightforward calculation gives

$$\begin{aligned}\eta_{CH} &= \int_{M_t}^{M_{xc}} \left[\beta_k M_t^{\beta_k} x^{-1-\beta_k} + \delta\left(x - M_{xc}\right)\left(\frac{M_t}{M_{xc}}\right)^{\beta_k}\right] \kappa \left(\frac{x}{M_t}\right)^{\alpha_k} dx \\ &= \kappa\beta_k M_t^{\beta_k-\alpha_k} \int_{M_t}^{M_{xc}} x^{-1-(\beta_k-\alpha_k)} dx + \frac{\kappa M_t^{\beta_k-\alpha_k}}{M_{xc}^{\beta_k}} \int_{M_t}^{M_{xc}} x^{\alpha_k}\delta(x - M_{xc})dx. \end{aligned} \tag{8}$$

We have then to distinguish between the cases $\beta_k \neq \alpha_k$ and $\beta_k = \alpha_k$.

2.1 Case $\beta_k \neq \alpha_k$

Setting $\beta_k \neq \alpha_k$, we use in the last integral of equation (8) that

$$\int_s^t f(x)\delta(x-y)dx = f(y)[u(y-s) - u(y-t)],$$

where

$$u(x) := \begin{cases} 1, & \text{if } x > 0 \\ 0, & \text{if } x < 0 \\ 0.5 & \text{if } x = 0 \end{cases}$$

is the unit step function. We then get

$$\begin{aligned}\eta_{CH} &= \frac{\kappa\beta_k}{\beta_k - \alpha_k} - \frac{\kappa\beta_k}{\beta_k - \alpha_k}\left(\frac{M_t}{M_{xc}}\right)^{\beta_k-\alpha_k} + \frac{\kappa}{2}\left(\frac{M_t}{M_{xc}}\right)^{\beta_k-\alpha_k} \\ &= \frac{\kappa\beta_k}{\beta_k - \alpha_k} - \frac{\kappa(\beta_k + \alpha_k)}{2(\beta_k - \alpha_k)}\left(\frac{M_t}{M_{xc}}\right)^{\beta_k-\alpha_k}. \end{aligned} \tag{9}$$

This shows that, when $\beta_k \neq \alpha_k$, the branching ratio η_{CH} of the ETAS-CH model is obtained as the classical one $\eta_{GR} = \frac{\kappa\beta_k}{\beta_k - \alpha_k}$ minus the quantity

$$\eta_{res} = \frac{\kappa(\beta_k + \alpha_k)}{2(\beta_k - \alpha_k)} \left(\frac{M_t}{M_{xc}}\right)^{\beta_k - \alpha_k}, \tag{10}$$

which is positive (negative) for $\beta_k > \alpha_k$ ($\beta_k < \alpha_k$). The relative graphical representation is given in Fig. 1, where η_{res} and η_{CH} are plotted against α_k and the ratio $\frac{M_t}{M_{xc}}$, for a fixed β_k both $<$ and $> \alpha_k$. By looking at the upper panels, corresponding to the case $\beta_k < \alpha_k$, we can observe that η_{res} and η_{CH} have a similar decreasing trend with α_k, while an opposite trend with respect to the ratio $\frac{M_t}{M_{xc}}$. Still, the latter's velocity rate is for both the quantities very slow. The bottom panels in Fig. 1 show instead that when $\beta_k > \alpha_k$, η_{res} and η_{CH} have an opposite monotonicity with respect to both the two variables they are plotted against.

The asymptotics for the cutoff magnitude to 0 or to infinity analytically confirm the evidence shown in the above figure. Explicit computations give

$$\lim_{M_{xc}\to M_t} \eta_{res} = \frac{\kappa(\beta_k + \alpha_k)}{2(\beta_k - \alpha_k)} = \frac{1}{2}\eta_{GR} + \frac{\kappa\alpha_k}{2(\beta_k - \alpha_k)}, \tag{11}$$

from which

$$\lim_{M_{xc}\to M_t} \eta_{CH} = \frac{1}{2}\eta_{GR} - \frac{\kappa\alpha_k}{2(\beta_k - \alpha_k)}. \tag{12}$$

The above quantity is always smaller than η_{GR}. In fact, if $\beta_k > \alpha_k$ ($\beta_k < \alpha_k$), the inequality

$$-\frac{1}{2}\eta_{GR} > \frac{\kappa\alpha_k}{2(\beta_k - \alpha_k)} \tag{13}$$

holds true if and only if $\beta_k < \alpha_k$ ($\beta_k > \alpha_k$), that is, there is no consistency with the conditions on the order relation between β_k and α_k. Still, we stress that only the hypothesis of $\beta_k > \alpha_k$ subsists for η_{GR} to exist.

In the limit for $M_{xc} \to \infty$ it holds instead

$$\lim_{M_{xc}\to\infty} \eta_{res} = \begin{cases} 0, & \text{if } \beta_k > \alpha_k, \\ -\infty, & \text{if } \beta_k < \alpha_k \end{cases} \quad \Leftrightarrow \quad \lim_{M_{xc}\to\infty} \eta_{CH} = \begin{cases} \eta_{GR}, & \text{if } \beta_k > \alpha_k, \\ +\infty, & \text{if } \beta_k < \alpha_k. \end{cases} \tag{14}$$

This shows that, for large M_{xc} and $\beta_k > \alpha_k$, the branching ratio η_{CH} has the same formulation of η_{GR}, as expected.

2.2 Case $\beta_k = \alpha_k$

If $\beta_k = \alpha_k$, formulation (8) becomes

$$\eta_{CH,\,\beta_k=\alpha_k} = \kappa\beta_k \int_{M_t}^{M_{xc}} x^{-1}dx + \frac{\kappa}{M_{xc}^{\beta_k}} \int_{M_t}^{M_{xc}} x^{\beta_k}\delta(x - M_{xc})dx = \frac{\kappa}{2} - \kappa\beta_k \ln\frac{M_t}{M_{xc}}, \tag{15}$$

whose graphical representation is given in Fig. 2 and shows that $\eta_{CH,\,\beta_k=\alpha_k}$ increases with the increase of both $\dfrac{M_t}{M_{xc}}$ and $\beta_k = \alpha_k$.

In this case, it is easy to see that

$$\lim \eta_{CH,\beta_k=\alpha_k} = \begin{cases} \infty, & \text{if } M_{xc} \to \infty \\ \dfrac{\kappa}{2}, & \text{if } M_{xc} \to M_t. \end{cases} \tag{16}$$

The previous results highlight that the condition $\beta_k > \alpha_k$, essential for the classical ETAS-GR case to guarantee the finiteness of the integral (4) (related to the non-explosion of the seismic sequence), is not required in the ETAS-CH modeling, as for the ETAS-TGR. This is what expected, in fact the CH law introduces a sharp upper cutoff to the magnitudes.

2.3 Criticality

As anticipated in Section 1, in the case of self exciting epidemic-type models, the critical parameter of the process coincides with the branching ratio, independently of the explicit formulation adopted for the magnitudes, as long as it is independent of space and time (i.e., the rate of the model is space-time-magnitude separable). It follows that the stability of the seismic process modeled through ETAS-CH is guaranteed by setting $\eta_{CH} < 1$, like it happens for ETAS-TGR and ETAS-GR (Zhuang et al. 2013). In the paper by Spassiani (2021) it is shown that, when $\beta_k > \alpha_k$, the non-explosion condition is less restrictive for the ETAS-TGR than for the ETAS-GR case, as $\eta_{GR} > \eta_{TGR}$. This inequality holds true also when substituting the branching ratio in the right-hand side (RHS) of this latter inequality with η_{CH}. In fact, as we explained before, the quantity η_{res} in (10) is positive when β_k is larger than α_k.

In the case of ETAS-CH, the parameter that mainly controls the branching ratio to be less than 1 is κ. This is shown in Fig. 3, where η_{CH} is plotted versus the difference $\beta_k - \alpha_k$, for four pairs (κ, β_k) and, in each of them, for four values of the ratio $\dfrac{m_t}{m_{xc}}$. We kept the y-scale fixed, and this highlights that the highest variability is observed between left and right panels, which differ for the value of κ indeed. The figure also shows that η_{CH} decreases with $\beta_k - \alpha_k$ and its rate of decrease is controlled by the ratio $\dfrac{m_t}{m_{xc}}$: the higher this latter, the slower the decrease. We stress that in this case we use and display the magnitudes (small letters m) instead of the seismic moments (capital letters M): this will be done also hereafter just as a "visualization" chioce for the plots to be more immediately understandable and more easily interpretable.

3 COMPARISON RESULTS

We now turn to the comparison of the seismic processes modeled through ETAS-GR, ETAS-TGR and ETAS-CH. To do that, we firstly focus on the branching ratios η_{GR}, η_{TGR} and η_{CH}, respectively

defined in (5), (6)-(7) and (9)-(15). For the sake of simplicity, hereafter we will set $m_c \equiv m_{xc}$ (or, equivalently, $M_c \equiv M_{xc}$).

The reciprocal relation between the branching ratios from ETAS-TGR and ETAS-CH is shown in Figures 4, 5 and 6. In the first one, the difference $\eta_{TGR} - \eta_{CH}$ of the quantities defined in (6) and (9) is plotted against $\beta_k - \alpha_k$, for a fixed pair $\left(\beta_k, \frac{m_t}{m_{xc}}\right)$ and two values of κ. This difference is shown to be very small, in fact it remains below $7 \cdot 10^{-2}$ also for the highest κ. Besides, the range of the y-axis is very narrow. This result highlights that the two branching ratios are close to each other, the smaller the κ value the lower their difference. It is what expected, as both the two FMDs introduce a rapid decay to the magnitude distribution: the only difference is that CH has a hard cutoff, while TGR has a soft taper. The ETAS-TGR process is expected to have a higher number of stronger events than ETAS-CH, and this is more evident when the κ parameter, which represents the productivity of aftershocks, is higher. We stress that we come to the same conclusions by using also different pairs of $\left(\beta_k, \frac{m_t}{m_{xc}}\right)$. More precisely, for a higher ratio $\frac{m_t}{m_{xc}}$ the difference falls below $4.5 \cdot 10^{-2}$, while it decreases with a higher β_k: still, the conclusions are the same. In Fig. 5, we show the contour plot of the difference $\eta_{TGR} - \eta_{CH}$ as a two-variables function of α_k and κ, for three values of β_k (each in one of the three lines), and $\beta_k > \alpha_k$ in the left panels while $\beta_k < \alpha_k$ in the right ones. We can see again that the difference is overall very small: it is larger for $\beta_k < \alpha_k$ than for $\beta_k > \alpha_k$, and this is quite independent of the β_k parameter value; finally, it becomes close to 0 in correspondence of smaller α_k and κ.

The case $\beta_k = \alpha_k$ is instead illustrated in Fig. 6, where we plot the difference $\eta_{TGR,\,\beta_k=\alpha_k} - \eta_{CH,\,\beta_k=\alpha_k}$ of the branching ratios defined in (7) and (15), versus the parameter κ. A linear increasing trend is observed, and this agrees with what is shown in Fig. 4 at the x-point $= 0$, where the line corresponding to the highest κ is above the other one. In agreement with the results obtained before, the difference remains small (here, smaller than $3.5 \cdot 10^{-2}$ in correspondence of the highest κ considered). We stress that, by using different values of the parameters, we obtained that for a higher β_k this difference becomes even smaller, while it does not change with the ratio $\frac{m_t}{m_{xc}}$. As expected, also in this case we can draw the same conclusions.

In Fig. 7 we finally plot the three branching ratios η_{GR}, η_{TGR} and η_{CH} together, to have an overall comparison. We can observe that the variation of η_{CH} and η_{TGR} with respect to their parameters is very slow, indeed, their ratio is almost coincident for the scale used; we stress that the latter has been chosen such as to allow to plot η_{GR} in the same figure. The non-explosion of the process is far more restrained when ETAS is embedded with CH or TGR rather than with GR. The latter is always above the former two, and they approach each other when $\beta_k - \alpha_k$ becomes larger. Again, we notice that the relative position between η_{CH} or η_{TGR} and η_{GR} is strongly controlled by the κ parameter: the higher the latter,

the greater the distance between the curves. This is more evident when the difference $\beta_k - \alpha_k$ is small. On the other hand, the influence of the b-value is quite unrelevant (see top right panel of Fig. 7). We underline that the curves corresponding to η_{GR} are plotted only for $\beta_k > \alpha_k$, since this branching ratio exists only when this condition is satisfied.

3.1 Simulations

A simulation analysis has been performed to study and compare ETAS-GR, ETAS-TGR and ETAS-CH realistic synthetic seismic sequences, such to highlight differences in the main features of the processes, like the number of aftershocks and background events, the magnitude distribution and the temporal evolution.

To obtain the synthetic catalogs, for each process of the two ETAS-TGR and ETAS-CH we first generate three synthetic magnitude sets of fixed cardinality $\bar{N} = 10000$, with the parameters $\alpha_k = 0.65$ and respectively $\beta_k = (0.74, 0.65, 0.59)$, that is, corresponding to the cases $\beta_k >, =, < \alpha_k$. For the ETAS-GR process we instead generate $\bar{N}$ synthetic magnitudes with $\alpha_k = 0.65 < \beta_k = 0.74$, since this condition is necessary in this case to guarantee the finiteness of the process. We specifically use the method for the inversion of the exponential cumulative distribution function. For TGR-distributed magnitudes, we adopt the competing risk approach proposed by Vere-Jones et al. (2001) and well described in Kagan & Schoenberg (2001). We stress that we are fixing here the number $\bar{N}$ of simulated events and, for the sake of simplicity, we will consider hereafter only the pure-temporal ETAS process.

Once obtained the seven synthetic sets of $\bar{N}$ magnitudes each, we correspondingly produce the synthetic pure-temporal earthquake catalogs by adapting the algorithm for the pure-temporal ETAS model proposed by Ogata on the basis of the thinning method for the simulation of point processes (`http://www.ism.ac.jp/~ogata/Ssg/ssg_softwaresE.html`, Lewis & Shedler (1979); Musmeci & Vere-Jones (1992); Ogata (1981, 1998)). Regarding the background and the temporal components of the ETAS rate, we use the fixed set of parameters $(\mu, \kappa, c, p) = (0.79, 0.012, 0.038, 1.13)$, as estimated for the Italian catalog from January 2007 to December 2014 through the maximum likelihood estimation (MLE) technique. We also set the completeness threshold equals to 2.5, while the cutoff magnitudes (m_c for TGR and m_{xc} for CH) both equal to 6. These choices for the input parameters are arbitrary and do not affect the conclusions deduced from the analysis, in agreement with the evidences obtained from the sensitivity analysis we performed in the previous Section 3.

The algorithm we develop allows also to build the family tree of the generated synthetic sequences by means of an in-line routine based again on the thinning (sampling) procedure (Zhuang et al. 2002; Zhuang 2006). It precisely allows to label each event as background or triggered, and to associate

to the aftershocks the relative mother events. In particular, to identify the mother of the i^{th} event we search for the previous k^{th} event, $k \in [0, i-1]$, such that the ratio between the model's rate in k and the model's rate in $i-1$ is for the first time larger than a random number between 0 and 1.

The first result is illustrated in Fig. 8, where we compare the branching ratios estimated for the simulated ETAS-GR, ETAS-TGR and ETAS-CH processes (square, circle and "x" markers, respectively) and for the three cases $\beta_k <, =, > \alpha_k$. The plot shows that η_{TGR} and η_{CH} are in general close to each other, and become closer as the difference $\beta_k - \alpha_k$ increases. The two branching ratios are also inversely proportional to this latter difference: the higher it is, the lower they are. For the case $\beta_k > \alpha_k$, the estimated η_{GR} is instead higher than the other branching ratios, and this directly follows from the hypothesis of unbounded magnitudes on which the GR law relies.

In Fig. 9 we show instead the numbers of triggering and triggered events generated in the three synthetic processes for the three cases $\beta_k <, =, > \alpha_k$. More precisely, in the left column panels we show the ratio of background and aftershocks events over the total length of the catalog ($\bar{N}$ events). In the right column panels we insted plot the first generation triggered events. We can observe a similar behavior for ETAS-CH and ETAS-TGR, in which the numbers of total and first generation aftershocks decrease with $\beta_k - \alpha_k$. When this difference is negative, the percentage of triggered events over the total is $\sim 98.3\%$ and 98.6%, respectively for ETAS-CH and ETAS-TGR, diminishing to 88.9% and 90.1% when the two parameters are equal. Finally, if $\beta_k > \alpha_k$ we obtain 57.4% and 58.1%. The total number of aftershocks decreases of 45 and 14 moving $\beta_k - \alpha_k$ from negative to 0 and then to positive, for ETAS-CH, while of 17 and 58 for ETAS-TGR. This difference may be induced by the sharp and tapered cutoffs of the two FMDs. To interpret these results we resort to the meaning of the parameters: β_k controls the proportion of larger to smaller events (the lower it is, the higher is the proportion), while α_k is related to the aftershocks productivity. The case $\beta_k < \alpha_k$ can be interpreted as the situation in which the role of aftershocks productivity in the seismic process is more remarkable, we could say "more tangible", than that of the rate of larger to smaller events. Therefore, the effect is to observe a higher number of triggered events and a higher number of first generation aftershocks. Besides, the proportion of aftershocks over the total is higher and this is reflected in a higher branching ratio. The percentage of triggered events over the total for the ETAS-GR is instead $\sim 91\%$, interestingly comparable to the other processes when $\beta_k = \alpha_k$.

Fig. 10 shows the cumulative magnitude distributions of the ETAS-GR, ETAS-CH and ETAS-TGR simulated processes. The last two are characterized by a lower taper as long as the difference $\beta_k - \alpha_k$ increases. The curve corresponding to ETAS-GR falls between the other two obtained for $\beta_k \geq \alpha_k$: it retraces quite well the ETAS-TGR and ETAS-CH FMDs for $\beta_k > \alpha_k$ until a certain magnitude value (< 5) and then, for larger magnitudes, it approaches the tails obtained for $\beta_k \leq \alpha_k$.

The histograms of the aftershocks' number with respect to the magnitudes are instead given in Fig. 11 for ETAS-CH and ETAS-TGR, and in panel a) of Fig. 12 for ETAS-GR. By looking at these plots, we can observe that the relationship $<, =, >$ between β_k and α_k plays a role also in correspondence of small magnitudes: the higher these parameters' difference, the higher the number of small events. In this case, no relevant diversity can be appreciated between the three FMDs apart from the tail values: the dashed lines indicate the location of the last bin in each case and we can observe that, for the simulated processes we generated, the one embedded with CH has a shorter tail. The histogram for ETAS-GR (see panel a) of Fig. 12) has a longer tail despite it corresponds to $\beta_k > \alpha_k$, the case that produces the shortest ending bins in ETAS-CH and ETAS-TGR.

As we can see in Fig. 13, the temporal intervals covered by the fixed number $\bar{N}$ of events in the synthetic ETAS-TGR and ETAS-CH catalogs are far more extended when β_k becomes higher than α_k. In the case $\beta_k < \alpha_k$ the two processes end earlier and the histograms are unbalanced towards higher times: this agrees with the results shown in Spassiani (2021). At first glance, this could be quite counterintuitive, as $\beta_k > \alpha_k$ is the case of a lower number of stronger shocks, which are those expected to be more productive. However, the histogram shows that when $\beta_k > \alpha_k$ the sequence is more uniformely spread along the time interval, and the absence of strong peaks justifies the conclusion we can draw. The case of ETAS-GR is instead shown in panel b) of Fig. 12. Here the temporal interval is quite uniformely occupied, and its length is comparable to those of the other processes in correspondence of $\beta_k = \alpha_k$. This calls back the conclusions we deduced by observing Fig. 9.

To investigate also how much and how differently productive are the ETAS-GR, ETAS-CH and ETAS-TGR simulated processes, we finally generate a second group of seven synthetic catalogs by using the same parameters and procedures as before, but we do not fix now the number of events to be produced. We fix instead the temporal interval of simulation to 1 year. In Figures 14 and 12c) we show the aftershocks temporal frequency relative to these synthetic processes, again in correspondence of the three cases $\beta_k <, =, > \alpha_k$. As before, in the ETAS-GR case we produce the simulations only for $\beta_k > \alpha_k$. All the plots show a similar behavior, which is quite uniformely spread along the interval considered. In Fig. 15 we finally show the numbers of events simulated for all the cases in the fixed temporal window: in the specific set of synthetic catalogs plotted, they are comparable with the exception of the ETAS-TGR case for $\beta_k < \alpha_k$. However, this result is not significant because, when iteratively generating the synthetic catalogs for several times, we obtained randomly varying results. Instead, conclusions about the FMDs and background/aftershocks numbers are comparable to the previous simulation analysis.

4 DISCUSSION AND CONCLUSIONS

The aim of this paper has been to compare the seismic processes modeled through ETAS with GR-, TGR- and CH-distributed magnitudes through both a theoretical and a simulation analysis. To do that, we first explicitly derived some theoretical features and relevant quantities of the ETAS-CH model, such as the branching ratio and the stability conditions, in order to allow a straightforward comparison with ETAS-GR and ETAS-TGR processes, for which these quantities and conditions have already been studied in the literature (e.g., see Zhuang et al. (2012) and Spassiani (2021); see also Sornette & Werner (2005) and Zhuang et al. (2013) for the ETAS-GR with an upper cutoff). Like in the case of η_{TGR}, we obtained that η_{CH} exists for all pairs (β_k, α_k) and, when $\beta_k > \alpha_k$, it is smaller than the classical η_{GR}. The non-explosion of the ETAS-CH process is therefore guaranteed by less restrictive conditions than ETAS-GR. In the case of ETAS-CH, κ is the parameter that mainly controls the branching ratio to be less than 1. Furthermore, η_{CH} decreases with the difference $\beta_k - \alpha_k$ with a velocity rate mainly controlled by $\dfrac{m_t}{m_{xc}}$.

The branching ratios of ETAS-GR, ETAS-TGR and ETAS-CH models were then analyzed from a theoretical point of view to perform a direct comparison of the three processes. More precisely, we focused on the relative behavior and the sensitivity with respect to the parameters, as well as on their reciprocal relationship. Results highlighted that all η_{GR}, η_{TGR} and η_{CH} decrease with $\beta_k - \alpha_k$, and the parameter which controls their reciprocal velocity rate is κ. The two branching ratios η_{TGR} and η_{CH} decrease with a lower rate than η_{GR}, and this is more clearly visible when $\beta_k - \alpha_k$ is small; they are also very close to each other, as their difference remains very small (of the order of $\sim 10^{-2}$ or below) in all the reasonable range for the parameters values. This highlights that the two TGR and CH FDMs behave very similarly, as expected: they both account for the limited amount of energy available in a given spatiotemporal domain, the only diversity is that TGR allows to model the stronger magnitudes with a more taper decay (probability-dependent) instead of a sharp cutoff, which induces a clean break of the distribution tail.

In order to investigate differences and similarities in the three processes' numbers and time/magnitude distributions, we made an additional step consisting in the generation of seven synthetic catalogs of $\bar{N}$ fixed events each: in the case of both the processes ETAS-TGR and ETAS-CH, one for each of the three possibilities $\beta_k <, =, > \alpha_k$; while, in the case of ETAS-GR, only for $\beta_k > \alpha_k$ due to the stability reasons (see Section 3.1). These parameters and their relationships regulate indeed the various possible scenarios and calibrate the main features of the processes. We obtained that a higher number of triggered events and first generation aftershocks are observed when $\beta_k < \alpha_k$, in agreement with the interpretation of these parameters' meaning. Interestingly, the ETAS-GR case shows similarities with the other two when $\beta_k = \alpha_k$, and we plan to investigate in more detail such behavior in a future study.

The temporal length occupied by the synthetic catalogs with $\bar{N}$ fixed events is longer for ETAS-CH and ETAS-TGR when $\beta_k > \alpha_k$, the case in which the seismicity is more uniformely spread along time. Such uniformity is instead satisfied by all the processes when they are simulated by fixing the temporal window. In this case, also the productivity is almost comparable.

The final conlcusion that we can drawn from the study we carried out is that the TGR law could be the best choice in the FMD modeling, as it allows to account for the limited amount of energy in small spatiotemporal domains, and it regulates the number of strong events in a probabilistic manner, which lowers the bias on the parameters' estimation. At the same time, it shows a very similar behavior of the ETAS-CH model, thus sharing the same grounds it has, but with less rigidity.

5 FIGURES

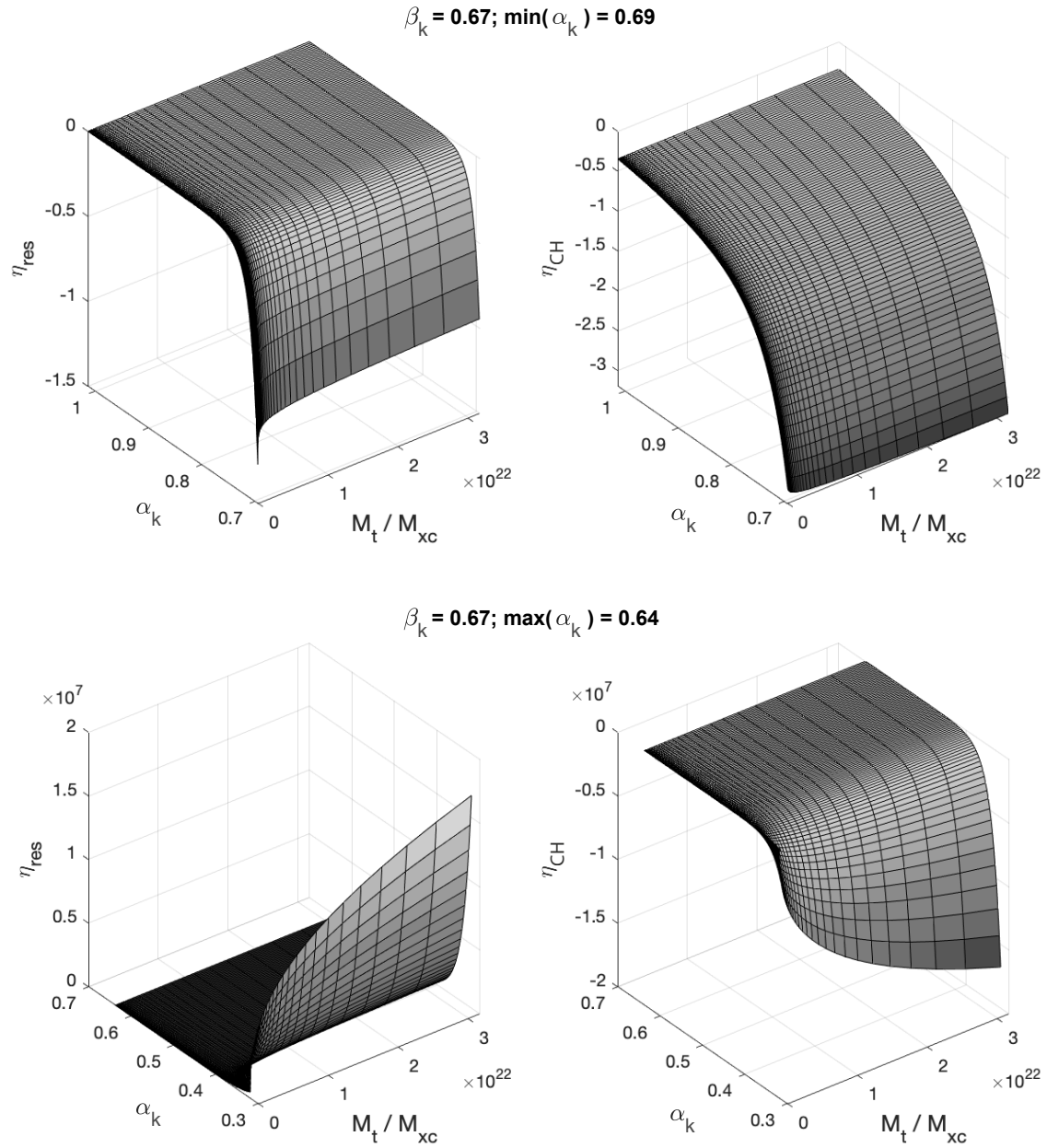

Figure 1. Three-dimensional representation of η_{res} (left column) and η_{CH} (right column) for varying α_k and $\frac{M_t}{M_{xc}}$, when $\beta_k < min(\alpha_k)$ (top) and $\beta_k > max(\alpha_k)$ (bottom).

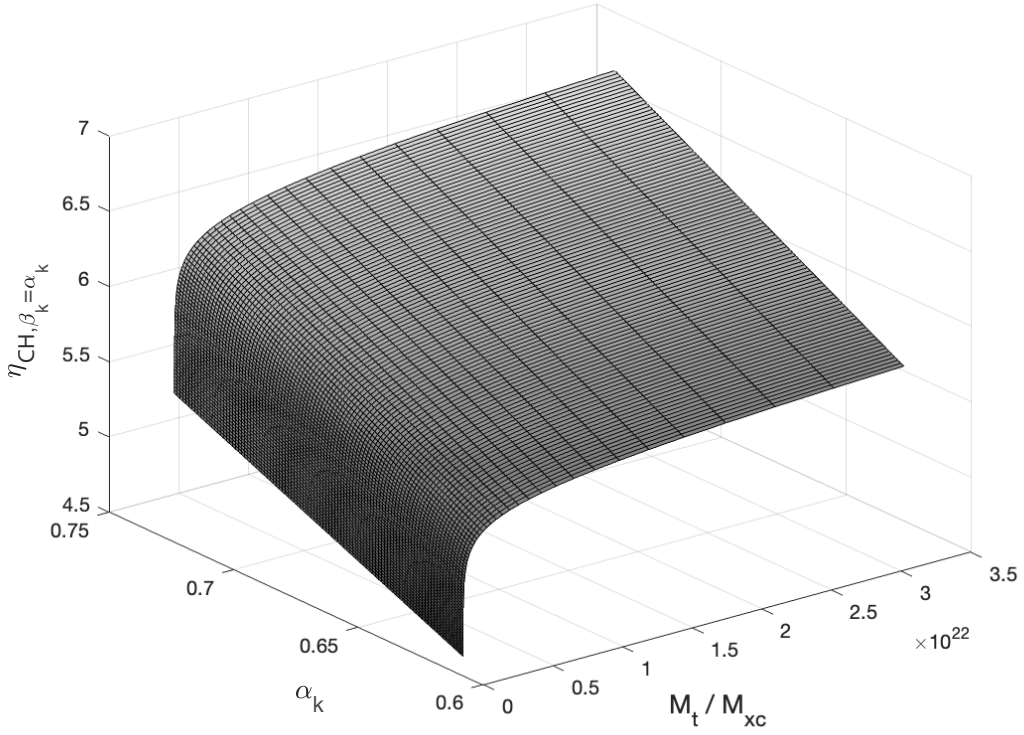

Figure 2. Three-dimensional representation of $\eta_{CH,\beta_k=\alpha_k}$ for varying $\beta_k = \alpha_k$ and $\frac{M_t}{M_{xc}}$.

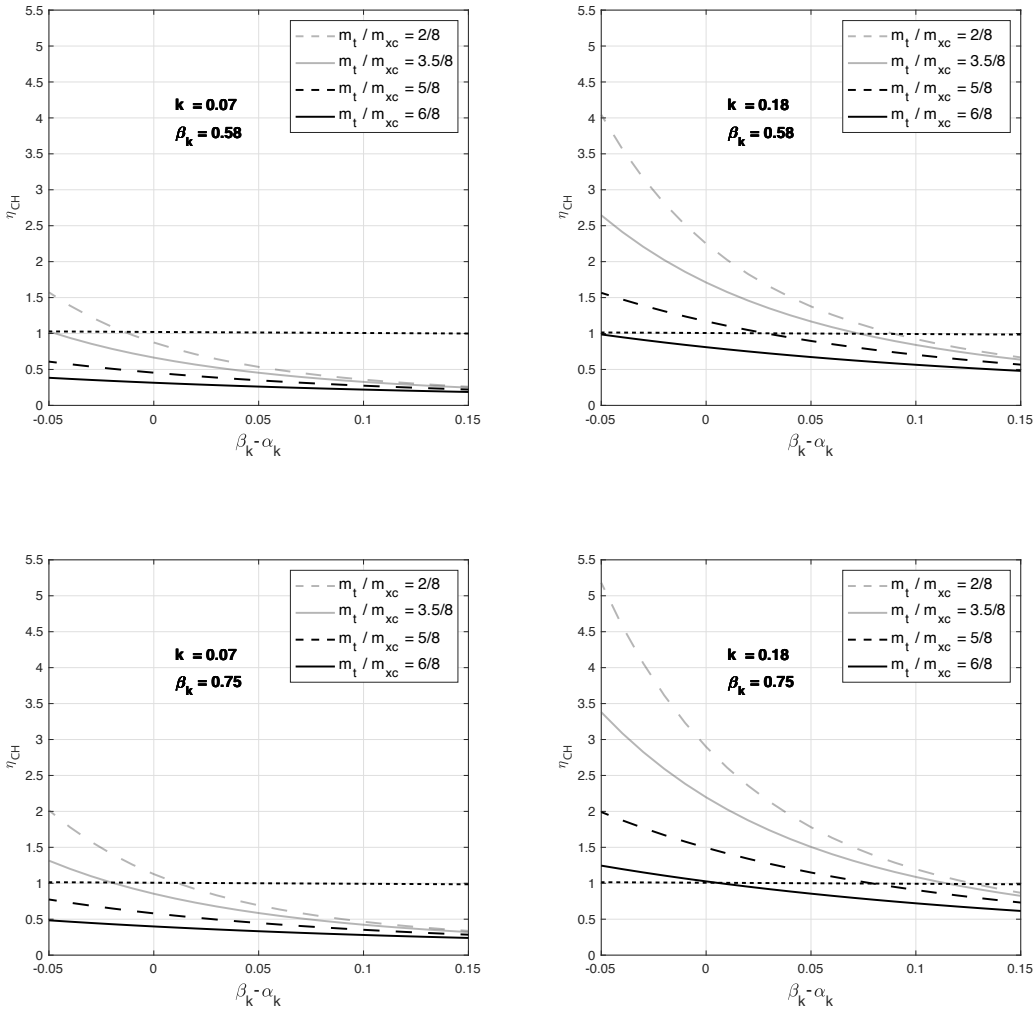

Figure 3. Branching ratio η_{CH} with respect to the difference $\beta_k - \alpha_k$ and several values of the ratio $\dfrac{m_t}{m_{xc}}$. Upper and lower panels correspond to $\beta_k = 0.58$ and $\beta_k = 0.75$, respectively. Left and right panels correspond instead to $\kappa = 0.07$ and $\kappa = 0.18$, respectively. The horizontal dotted line coincides with the value 1 and represents the threshold for the criticality (see the text for the details).

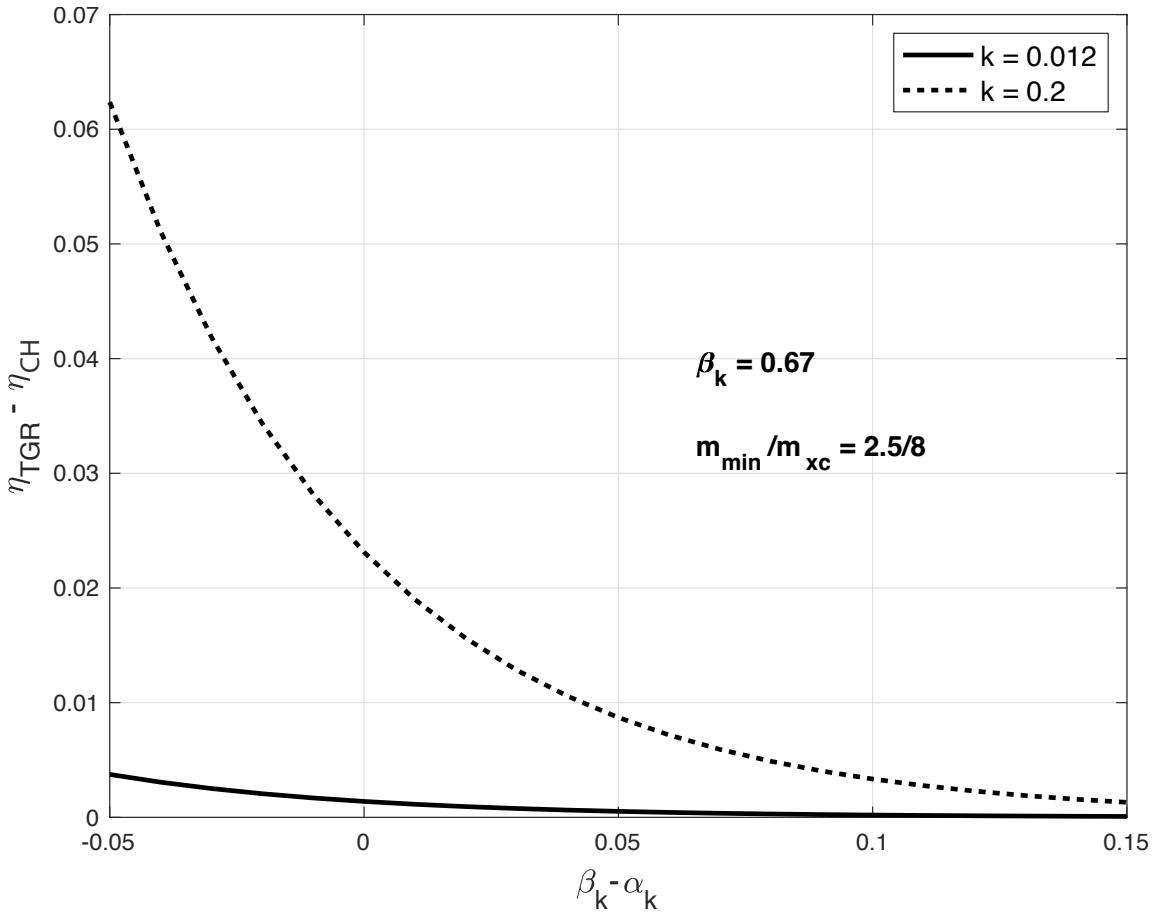

Figure 4. Difference $\eta_{TGR} - \eta_{CH}$ of the branching ratios defined in (6) and (9) versus $\beta_k - \alpha_k$, for a fixed pair $\left(\beta_k, \frac{m_t}{m_{xc}}\right)$ and two values of κ, indicated in the legend.

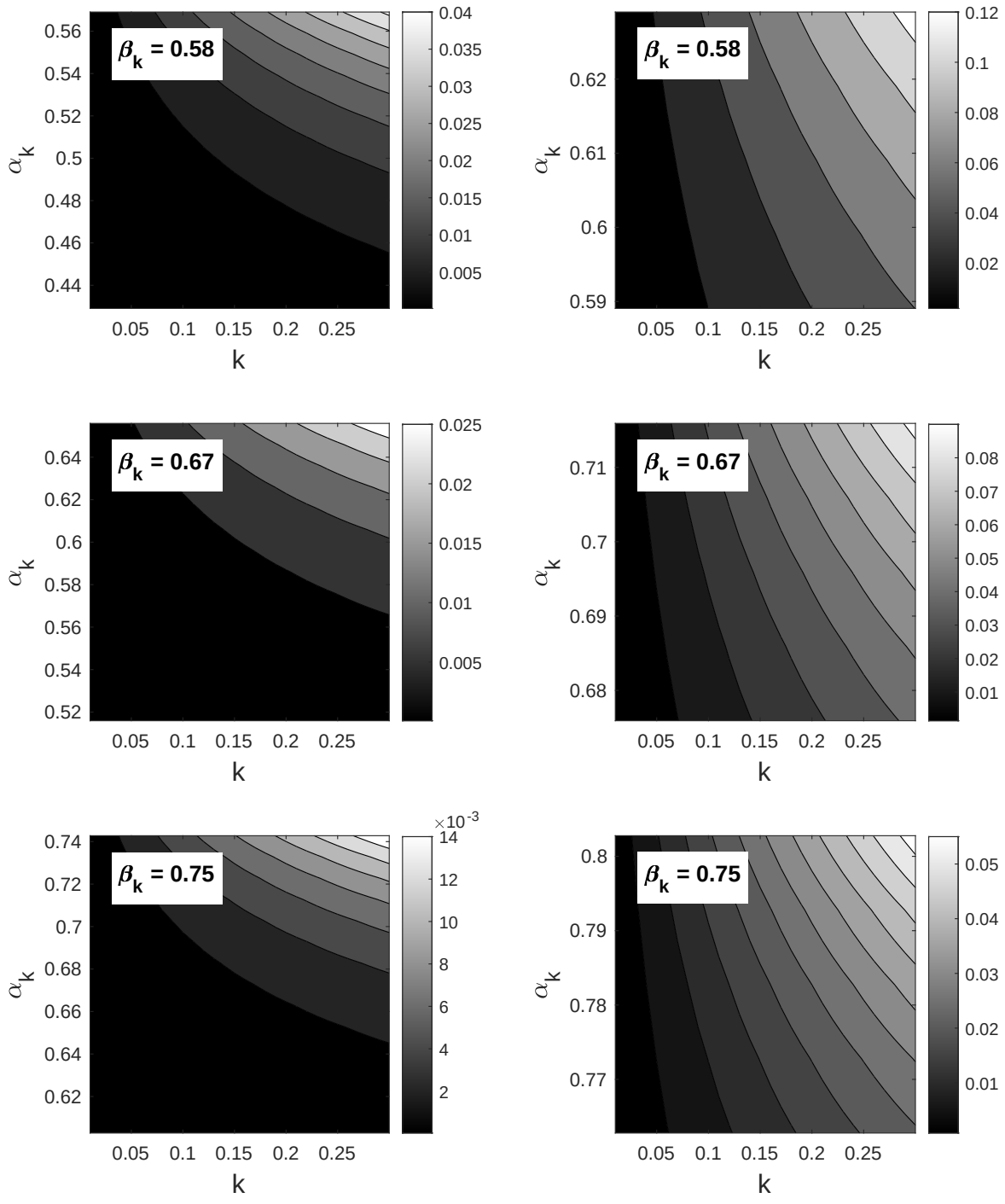

Figure 5. Contour plots of the difference $\eta_{TGR} - \eta_{CH}$ between the quantities defined in (6) and (9), as a two-variables function of α_k and κ. We set here $\dfrac{m_t}{m_{xc}} = \dfrac{2.5}{8}$ in all the paneles, and $\beta_k > \alpha_k$ ($\beta_k < \alpha_k$) in the left (right) ones.

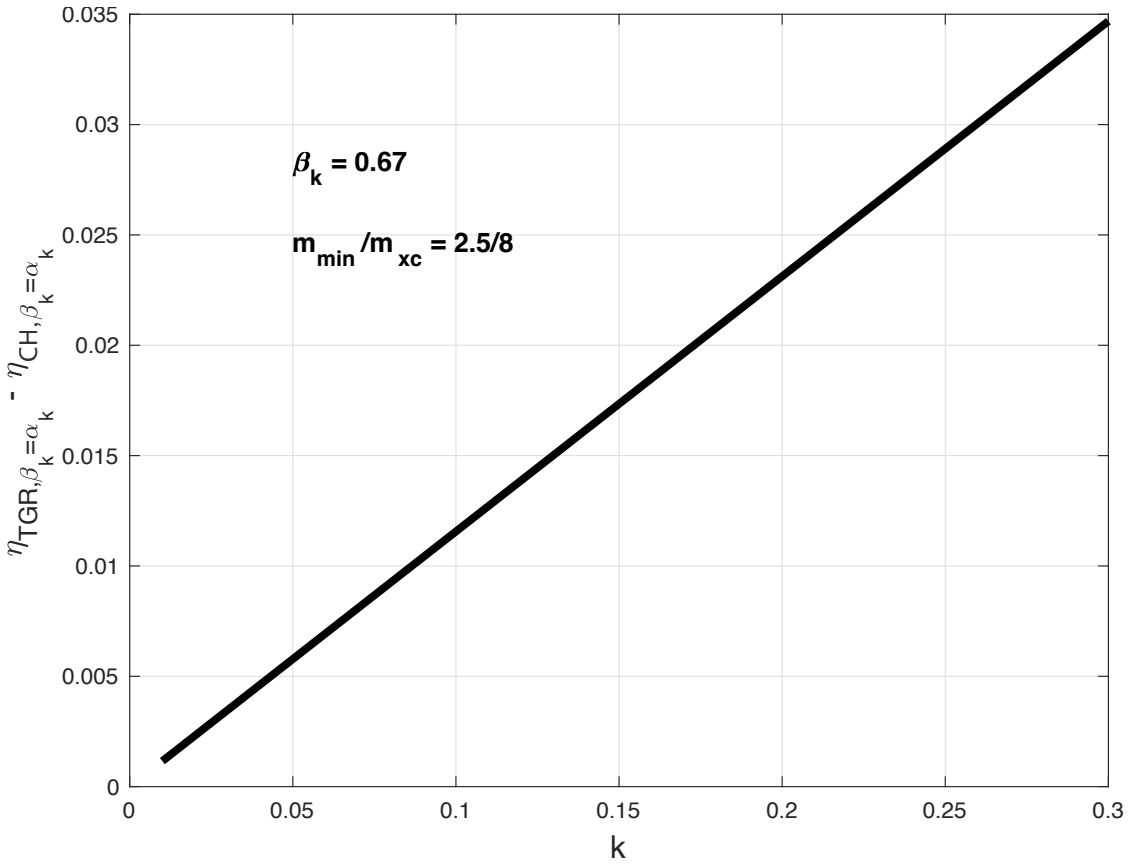

Figure 6. Difference $\eta_{TGR,\,\beta_k=\alpha_k} - \eta_{CH,\,\beta_k=\alpha_k}$ of the branching ratios defined in (7) and (15) for the case $\beta_k = \alpha_k$, versus the parameter κ, for a fixed pair $\left(\beta_k, \dfrac{m_t}{m_{xc}}\right)$.

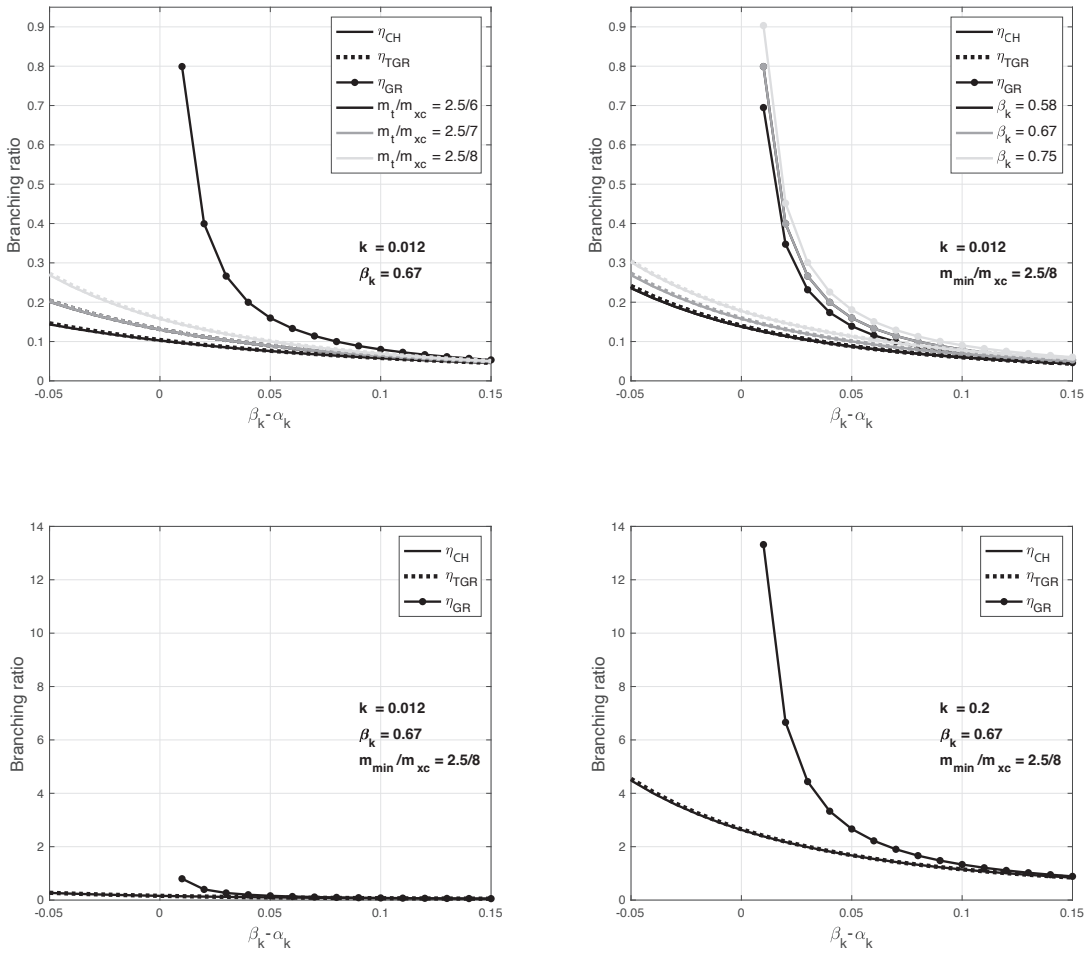

Figure 7. Overall comparison among η_{GR}, η_{TGR} and η_{CH}, as functions of the difference $\beta_k - \alpha_k$, for several values of their parameters, as indicated in the panels. Continuous, dotted and continuous-with-circles lines refer to η_{CH}, η_{TGR} and η_{GR} branching ratios, respectively. The first three items in the legend of the upper panels are just referred to the line styles, and can be associated to all the three gray-scaled colors. In the panels of each line we also fixed the y-axis to have an easier comparison.

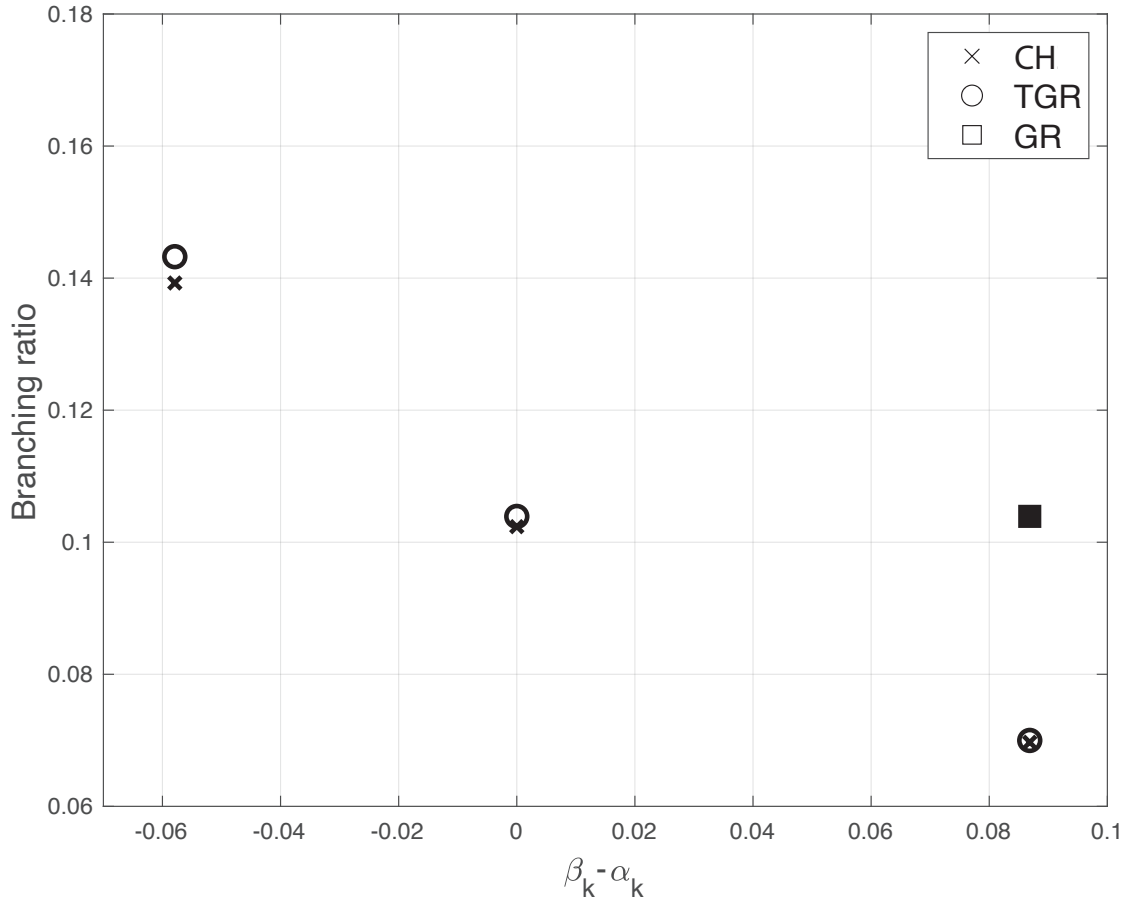

Figure 8. Branching ratios of the ETAS-CH ("x" marker), ETAS-TGR (circle marker) and ETAS-GR (square marker) simulated processes, and for the three cases of $\beta_k <, =, > \alpha_k$. The η_{GR} has been computed only for $\beta_k > \alpha_k$, since for the process ETAS-GR the latter condition is necessary to guarantee the non-explosion.

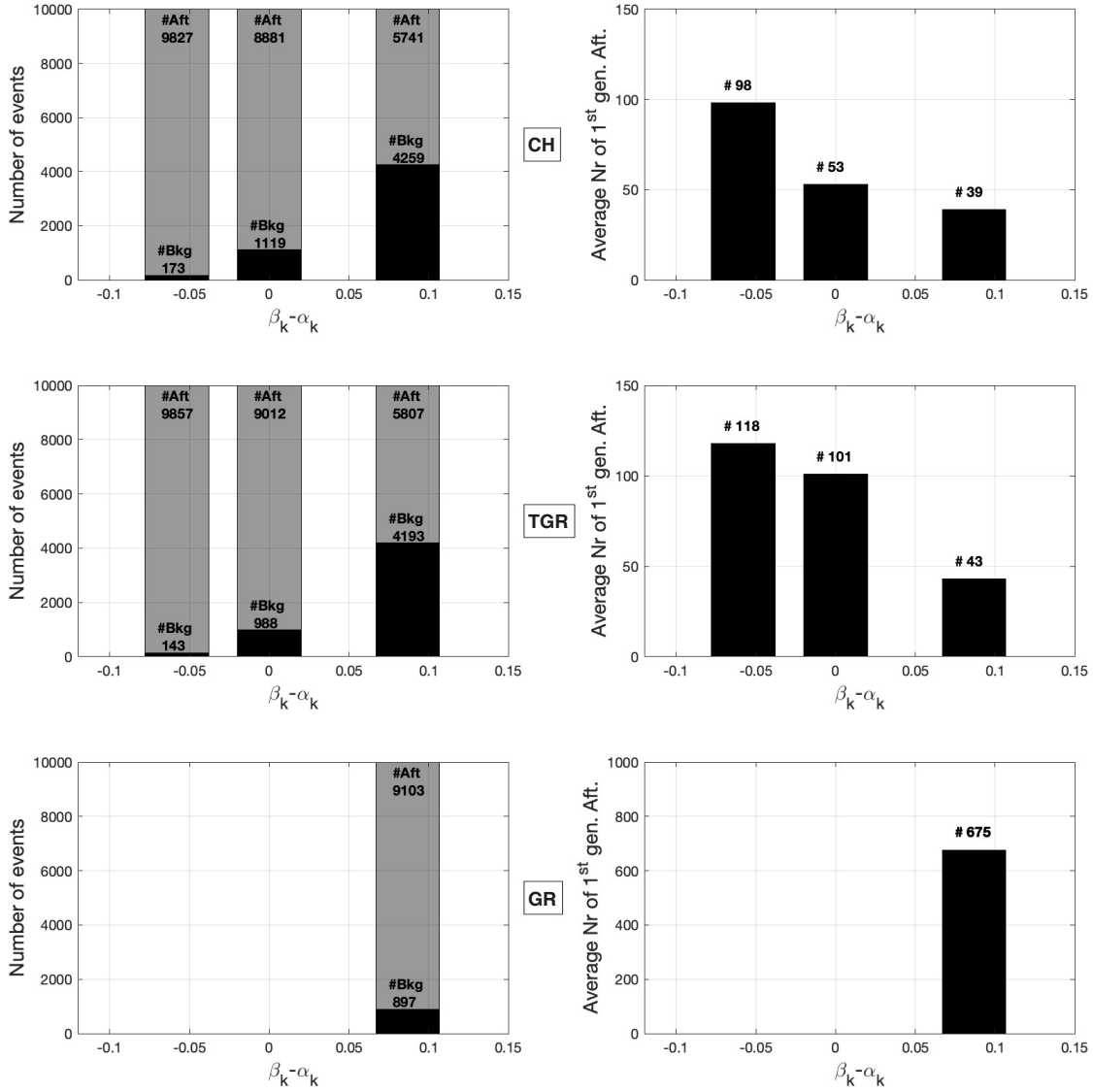

Figure 9. Events' number comparison of the ETAS-CH (first line panels), ETAS-TGR (second line panels) and ETAS-GR (third line panels) simulated processes. Specifically, the left panels contain the numbers of background events (#Bkg) and aftershocks (#Aft) (respectively solid and 50% trasparent colors), while the right panels show the average numbers of the first generation aftershocks. The numbers relative to ETAS-GR have been computed only for $\beta_k > \alpha_k$, since for this process the latter condition is necessary to guarantee the non-explosion.

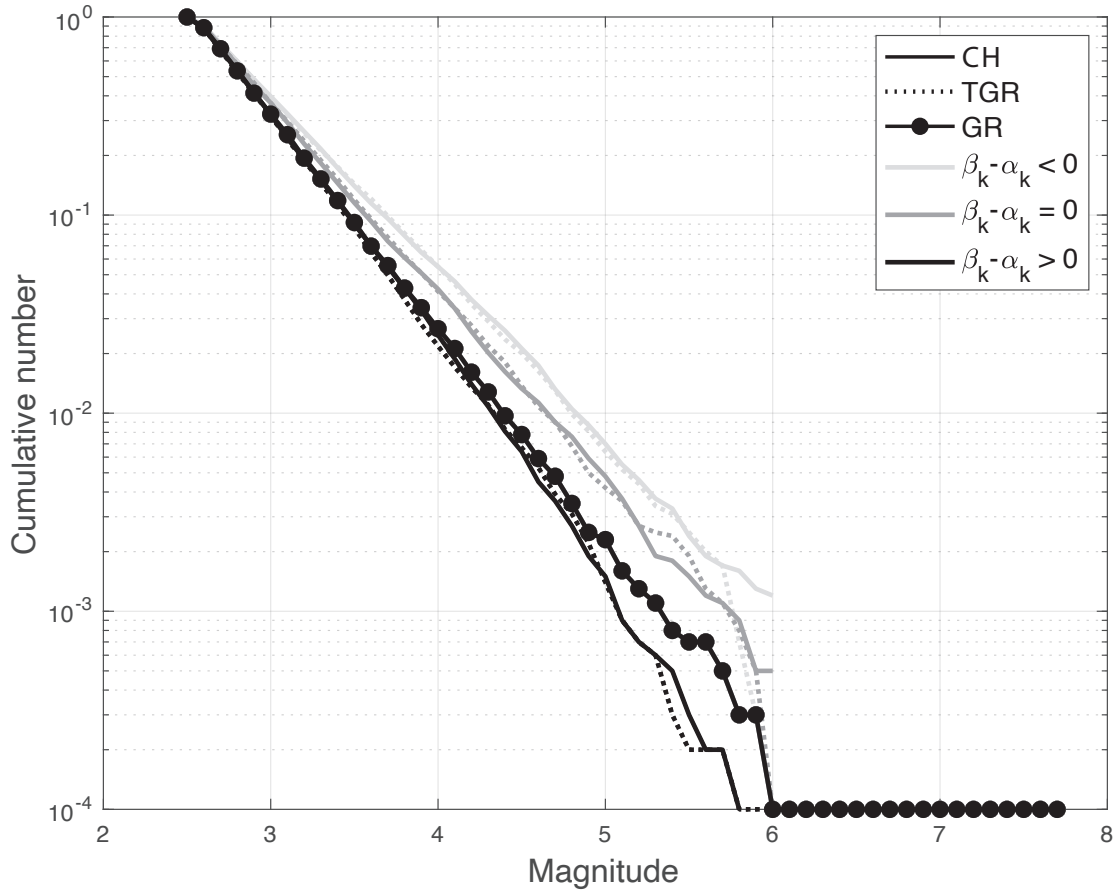

Figure 10. Magnitude cumulative distributions of the ETAS-CH (continuous line), ETAS-TGR (dotted line) and ETAS-GR (continuous-with-circles line) simulated processes, for the three cases of $\beta_k <, =, > \alpha_k$. The first three items in the legend are just referred to the line styles, and can be associated to all the three gray-scaled colors in the plot. The cumulative distribution relative to ETAS-GR has been computed only for $\beta_k > \alpha_k$, since for this process the latter condition is necessary to guarantee the non-explosion.

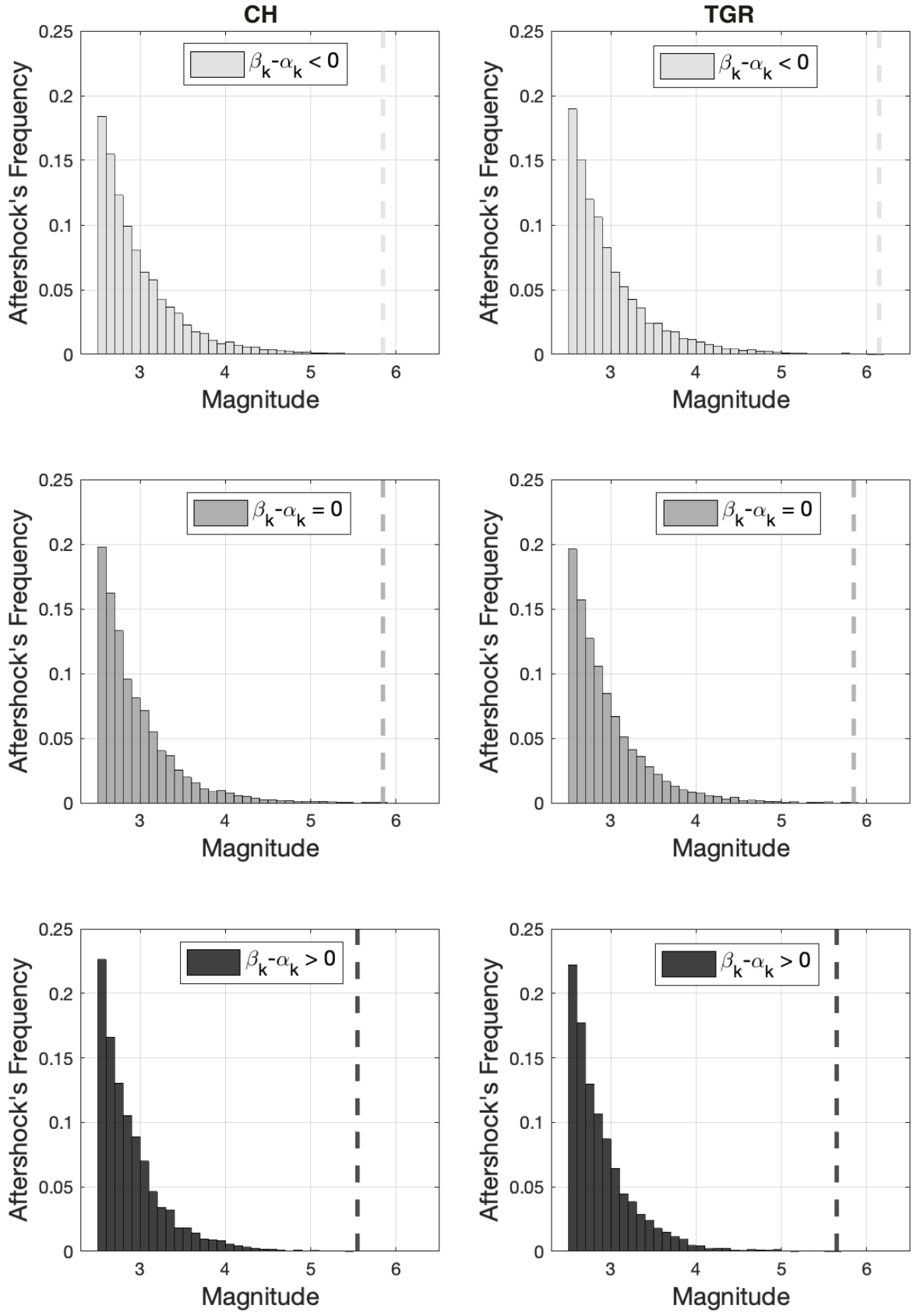

Figure 11. Frequencies of the aftershocks versus the magnitudes, relative to the ETAS-CH (left column panels) and ETAS-TGR (right column panels) simulated processes. Gray-scaled colors are used for $\beta_k <, =, > \alpha_k$ (from top to bottom panels). The vertical dashed lines correspond to the last non-empty bin occupied by the aftershocks' magnitude frequencies.

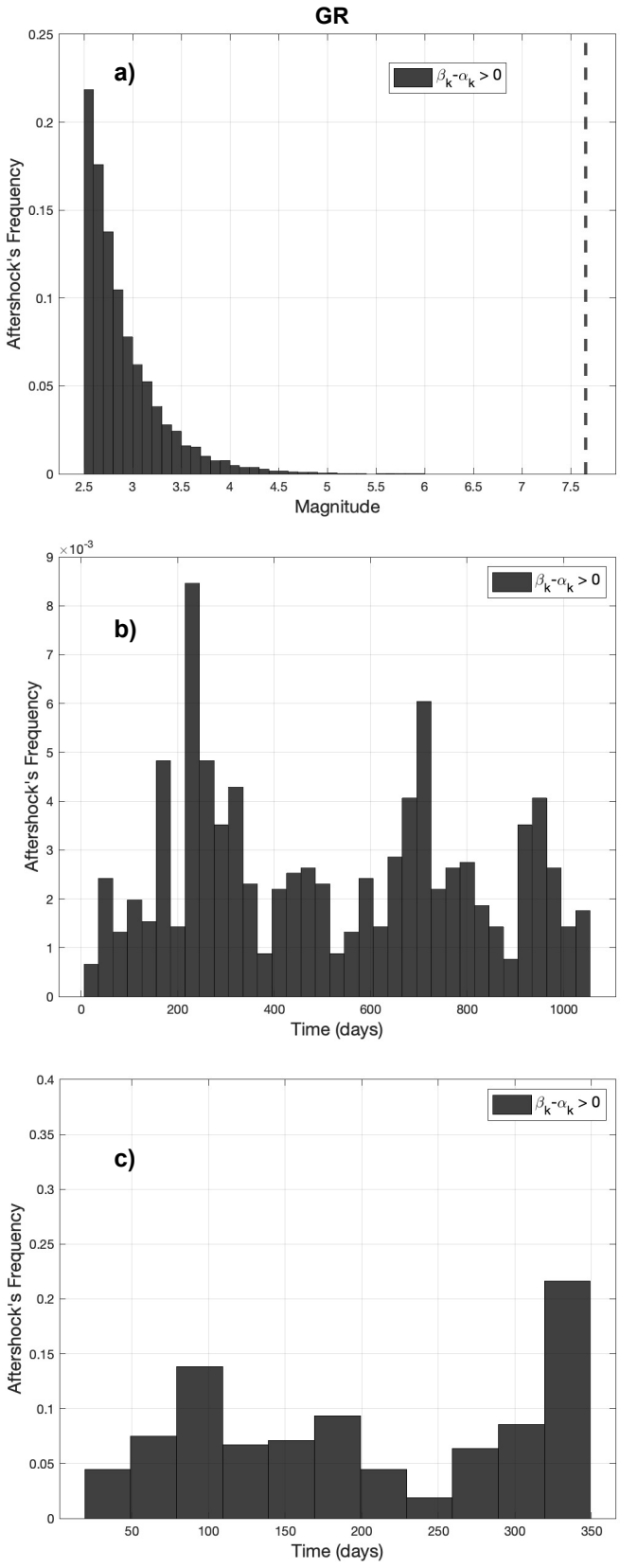

Figure 12. Results relative to the ETAS-GR simulated process. Panel a): frequency of the aftershocks versus the magnitudes; the vertical dashed line corresponds to the last non-empty bin occupied by the aftershocks' magnitude frequency. Panel b): temporal frequency of the aftershocks. Panel c): the same of panel b), but here simulations are obtained for a fixed temporal window of 1 year. In all the panels, only the case $\beta_k > \alpha_k$ is considered, since this condition is necessary to guarantee the non-explosion of the ETAS-GR process.

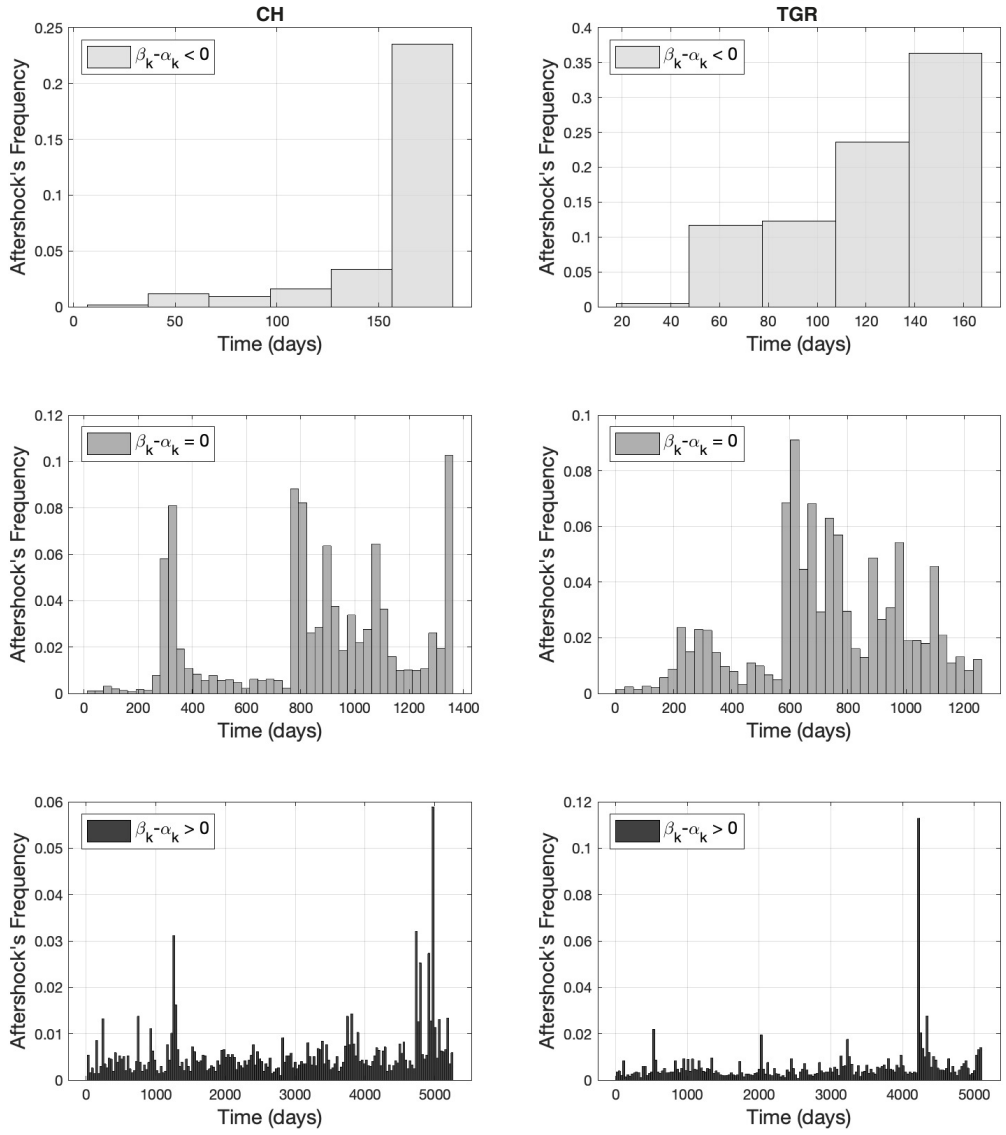

Figure 13. Temporal frequency of the aftershocks relative to ETAS-CH (left column panels) and ETAS-TGR (right column panels) simulated processes. Gray-scaled colors are used for $\beta_k <, =, > \alpha_k$ (from top to bottom panels).

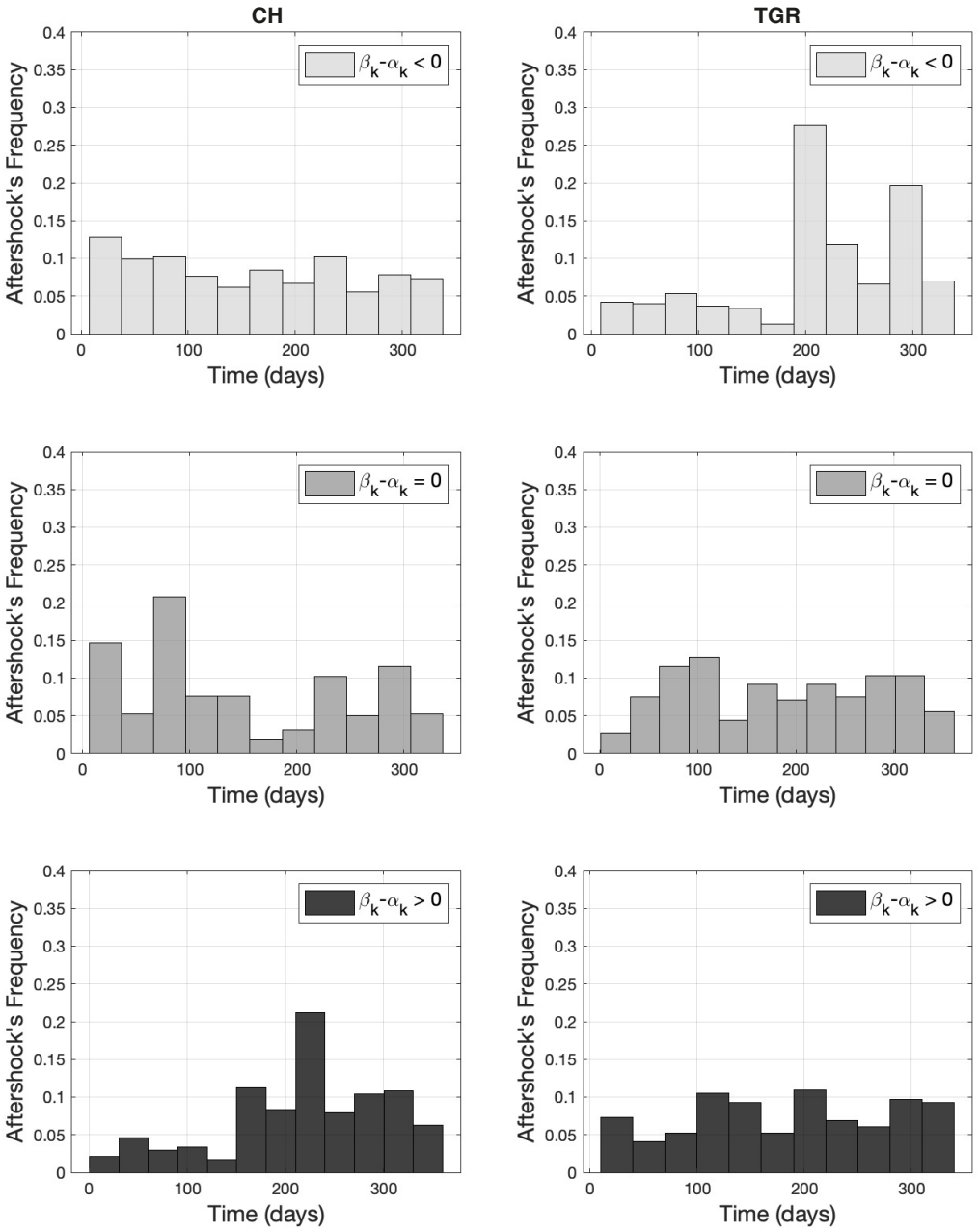

Figure 14. Temporal frequency of the aftershocks relative to ETAS-CH (left column panels) and ETAS-TGR (right column panels) simulated processes. Here simulations are obtained for a fixed temporal window of 1 year. Gray-scaled colors are used for $\beta_k <, =, > \alpha_k$ (from top to bottom panels).

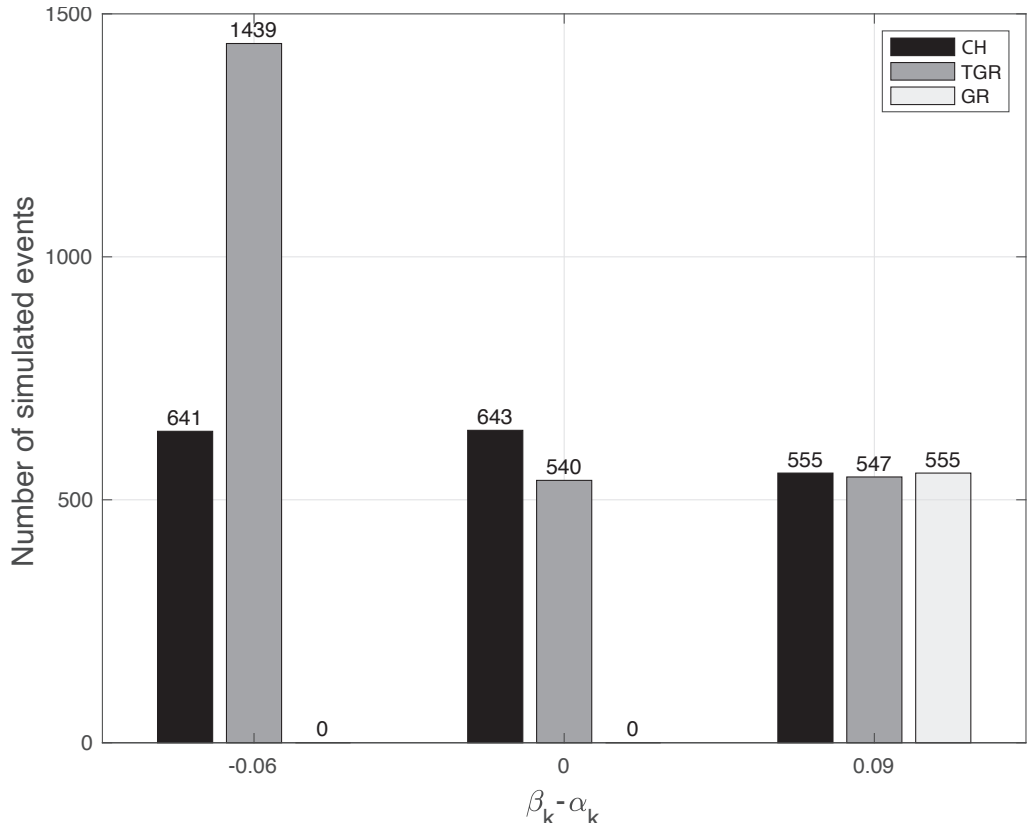

Figure 15. Numbers of events simulated for the ETAS-CH (black), ETAS-TGR (dark gray) and ETAS-GR (light gray) simulated processes, and for $\beta_k <, =, > \alpha_k$. Here simulations are obtained for a fixed temporal window of 1 year. We stress that we computed the number for the ETAS-GR process only in the case $\beta_k > \alpha_k$, since this condition is necessary to guarantee the non-explosion of the process.

DATA AVAILABILITY

The data underlying this article will be shared on reasonable request to the corresponding author.

ACKNOWLEDGMENTS

The authors are very thankful to Elham Shokrgozar for her useful help in the code to produce CH-distributed synthetic magnitudes. We also thank very much Chris Rollins and the other anonymous reviewer for their useful comments and suggestions.

REFERENCES

Arroyo-Solórzano, M. & Linkimer, L., 2021. Spatial variability of the b-value and seismic potential in Costa Rica, *Tectonophysics*, **814**, 228951.

Console, R. & Murru, M., 2001. A simple and testable model for earthquake clustering, *Journal of Geophysical Research: Solid Earth*, **106**(B5), 8699–8711.

Console, R., Murru, M., & Lombardi, A. M., 2003. Refining earthquake clustering models, *Journal of Geophysical Research: Solid Earth*, **108**(B10).

Field, E. H., Jordan, T. H., Page, M. T., Milner, K. R., Shaw, B. E., Dawson, T. E., Biasi, G. P., Parsons, T., Hardebeck, J. L., Michael, A. J., Weldon II, R. J., Powers, P. M., Johnson, K. M., Zeng, Y., Felzer, K. R., van der Elst, N., Madden, C., Arrowsmith, R., Werner, M. J., & Thatcher, W., 2017. A synoptic view of the third Uniform California Earthquake Rupture Forecast (UCERF3), *Seismological Research Letters*, **88**(5), 1259–1267.

Gutenberg, B. & Richter, C. F., 1944. Frequency of earthquakes in California, *Bull. Seismol. Soc. Am.*, **34**(8), 185–188.

Hussain, H., Shuangxi, Z., Usman, M., & Abid, M., 2020. Spatial Variation of b-values and their relationship with the fault blocks in the Western Part of the Tibetan Plateau and its surrounding areas, *Entropy*, **22**(9), 1016.

Ishibe, T. & Shimazaki, K., 2008. The Gutenberg-Richter Relationship vs. the Characteristic Earthquake Model: Effects of different sampling methods, *Bulletin of Earthquake Research Institute, University of Tokyo*, **83**, 131–151.

Ishibe, T. & Shimazaki, K., 2012. Characteristic earthquake model and seismicity around late Quaternary active faults in Japan, *Bulletin of the Seismological Society of America*, **102**(3), 1041–1058.

Kagan, Y., Bird, P., & Jackson, D., 2010. Earthquake Patterns in Diverse Tectonic Zones of the Globe, *Pure and Applied Geophysics*, **167**, 721–741.

Kagan, Y. Y., 2002. Seismic moment distribution revisited: I. Statistical results, *Geophys. J. Int.*, **148**(3), 520–541.

Kagan, Y. Y. & Schoenberg, F., 2001. Estimation of the Upper Cutoff Parameter for the Tapered Pareto Distribution, *J. Appl. Probab.*, **38**.

Kanamori, H., 1977. The energy release in great earthquakes, *J. Geophys. Res.*, **82**(20).

Lewis, P. W. & Shedler, G. S., 1979. Simulation of nonhomogeneous Poisson processes by thinning, *Naval research logistics quarterly*, **26**(3), 403–413.

Marzocchi, W., Spassiani, I., Stallone, A., & Taroni, M., 2020. How to be fooled searching for significant variations of the b-value, *Geophysical Journal International*, **220**(3), 1845–1856.

Montuori, C., Falcone, G., Murru, M., Thurber, C., Reyners, M., & Eberhart-Phillips, D., 2010. Crustal heterogeneity highlighted by spatial b-value map in the Wellington region of New Zealand, *Geophysical Journal International*, **183**(1), 451–460.

Musmeci, F. & Vere-Jones, D., 1992. A space-time clustering model for historical earthquakes, *Annals of the Institute of Statistical Mathematics*, **44**(1), 1–11.

Ogata, Y., 1981. On Lewis' simulation method for point processes, *IEEE transactions on information theory*, **27**(1), 23–31.

Ogata, Y., 1988. Statistical models for earthquake occurrences and residual analysis for point processes, *Journal of the American Statistical association*, **83**(401), 9–27.

Ogata, Y., 1998. Space-time point-process models for earthquake occurrences, *Annals of the Institute of Statistical Mathematics*, **50**(2), 379–402.

Schorlemmer, D., Wiemer, S., & Wyss, M., 2005. Variations in earthquake-size distribution across different stress regimes, *Nature*, **437**(7058), 539–542.

Sornette, D. & Werner, M. J., 2005. Constraints on the size of the smallest triggering earthquake from the epidemic-type aftershock sequence model, Båth's law, and observed aftershock sequences, *Journal of Geophysical Research: Solid Earth*, **110**(B8).

Spassiani, I., 2021. Stability of the Epidemic-Type Aftershock Sequence Model with Tapered Gutenberg-Richter Distributed Seismic Moments, *Bulletin of the Seismological Society of America*, **111**(1), 398–408.

Spassiani, I. & Marzocchi, W., 2021. An energy-dependent earthquake moment-frequency distribution, *Bulletin of the Seismological Society of America*, **111**(2), 762–774.

Tan, Y. J., Waldhauser, F., Tolstoy, M., & Wilcock, W., 2019. Axial Seamount: Periodic tidal loading reveals stress dependence of the earthquake size distribution (b value), *Earth and Planetary Science Letters*, **512**, 39–45.

Taroni, M., Selva, J., & Zhuang, J., 2021. Estimation of the tapered gutenberg-richter distribution parameters for catalogs with variable completeness: An application to the atlantic ridge seismicity, *Applied Sciences*, **11**(24), 12166.

Vere-Jones, D., Robinson, R., & Yang, W., 2001. Remarks on the accelerated moment release model: problems of model formulation, simulation and estimation, *Geophys. J. Int.*, **144**(3), 517–531.

Wesnousky, S. G., 1994. The Gutenberg-Richter or characteristic earthquake distribution, which is it?, *Bulletin of the Seismological Society of America*, **84**(6), 1940–1959.

Westerhaus, M., Wyss, M., Yilmaz, R., & Zschau, J., 2002. Correlating variations of b values and crustal deformations during the 1990s may have pinpointed the rupture initiation of the M w= 7.4 Izmit earthquake of 1999 August 17, *Geophysical Journal International*, **148**(1), 139–152.

Yaghmaei-Sabegh, S. & Ebrahimi-Aghabagher, M., 2017. Near-field probabilistic seismic hazard analysis with characteristic earthquake effects, *Natural hazards*, **87**(3), 1607–1633.

Yaghmaei-Sabegh, S. & Ostadi-Asl, G., 2021. Estimating of the b-Value Based on the Characteristic Earthquake Model, *Journal of Earthquake and Tsunami*, **15**(03), 2150015.

Zhuang, J., 2006. Second-order residual analysis of spatiotemporal point processes and applications in model evaluation, *Journal of the Royal Statistical Society: Series B (Statistical Methodology)*, **68**(4), 635–653.

Zhuang, J., 2012. Long-term earthquake forecasts based on the epidemic-type aftershock sequence (ETAS) model for short-term clustering, *Research in Geophysics*, **2**(1), e8–e8.

Zhuang, J., Ogata, Y., & Vere-Jones, D., 2002. Stochastic declustering of space-time earthquake occurrences, *Journal of the American Statistical Association*, **97**(458), 369–380.

Zhuang, J., Harte, D., Werner, M., Hainzl, S., & Zhou, S., 2012. Basic Models of Seismicity: Temporal Models, *"Community Online Resource for Statistical Seismicity Analysis*.

Zhuang, J., Werner, M. J., & Harte, D. S., 2013. Stability of earthquake clustering models: Criticality and branching ratios, *Physical Review E*, **88**(6), 062109.